COMBUSTION SYNTHESIS/DYNAMIC DENSIFICATION OF TiC-Ni CERMETS

J.C. LaSalvia and M.A. Meyers
Department of Applied Mechanics and Engineering Sciences
University of California, San Diego
La Jolla, CA 92093

D.K. Kim
Korea Advanced Institute of Science and Technology
Yusong Gu, Taejon 205-701, Korea

Journal of MATERIALS SYNTHESIS and PROCESSING, Volume 2, Number 4, 1994, pp. 255-274

Journal of Materials Synthesis and Processing, Vol. 2, No. 4, 1994

Combustion Synthesis/Dynamic Densification of TiC—Ni Cermets

J. C. LaSalvia,[1] M. A. Meyers,[1,2] and D. K. Kim[1,3]

The Ti + C → TiC exothermic chemical reaction was utilized in conjunction with dynamic densification in a high-velocity forging machine to produce fully dense particulate TiC—Ni-based cermets. Nickel formed a quasi-continuous phase enveloping spheroidal TiC particles with an apparent diameter of 5 μm. The exothermic reaction between Ti and C resulted in the melting of the Ni particles. The microstructure of the product was characterized by optical, scanning, and transmission electron microscopy. The TiC phase is typically composed of one to several grains; interfacial bonding between TiC and Ni was found to be of a good quality (i.e., free of second phases). The nickel phase had a large grain size (> TiC), indicating that it had undergone recrystallization and grain growth after densification. Compressive tests revealed that fracture proceeds without significant debonding of Ni—TiC; the compressive strength is approximately 2.9 GPa, typical of conventionally processed cermets. Four-point bending tests revealed a strength (in tension) of 0.47 GPa.

KEY WORDS: Combustion synthesis; dynamic densification; cermets; titanium carbide; nickel binder.

1. INTRODUCTION

Interest in TiC-based cermets stems from the desire of the cutting-tool industry to find ways to reduce its dependence on WC—Co-based cermets, due to improved performance. WC—Co-based cermets are still widely used, especially in rough machining [4]. However, TiC-based cermets are gradually replacing WC—Co in rough machining [5, 7].

The fabrication of cermets typically involves traditional powder metallurgical techniques, in which the powder is densified through liquid-phase sintering, infiltration, or hot-pressing [6, 8]. This manufacturing process is highly reliable; however, it is both labor and energy intensive. Combustion synthesis is a materials processing technique which involves an exothermic chemical reaction [9, 10]. This process has been extensively developed in Russia by Merzhanov, Borovinskaya, and co-workers during the past 25 years [11–16]. These researchers have synthesized over 500 compounds, many of which are produced for industrial purposes. In the United States and Japan, researchers have been studying both fundamental aspects of the process and industrial applications [17–21]. One of the initial drawbacks of the combustion synthesis process has been that the final products can be highly porous. However, research in Russia, Japan, and the United States has shown that the final products can be densified immediately after the synthesis process by hot-pressing [17, 22–26], rolling [27, 28], extrusion [28], modified HIPing [19, 29, 30], and shock-wave compaction [31–33]. In addition, dense combustion synthesis products have been achieved through pressureless reactive sintering and casting [34, 37]. Dense ceramic and cermet pipe liners have been fabricated by combining combustion synthesis with centrifugal rolling [28].

An alternative manufacturing method that is potentially more cost effective (at least for simple shapes such as plates) and utilizes the combustion synthesis process in combination with a forging step to provide densification is described here. Impact forging has been suc-

[1] Department of Applied Mechanics and Engineering Sciences, University of California, San Diego, La Jolla, California 92093.
[2] To whom correspondence should be addressed.
[3] Korea Advanced Institute of Science and Technology, Taejon, Korea.

1064-7562/94/0700-0255$07.00/0

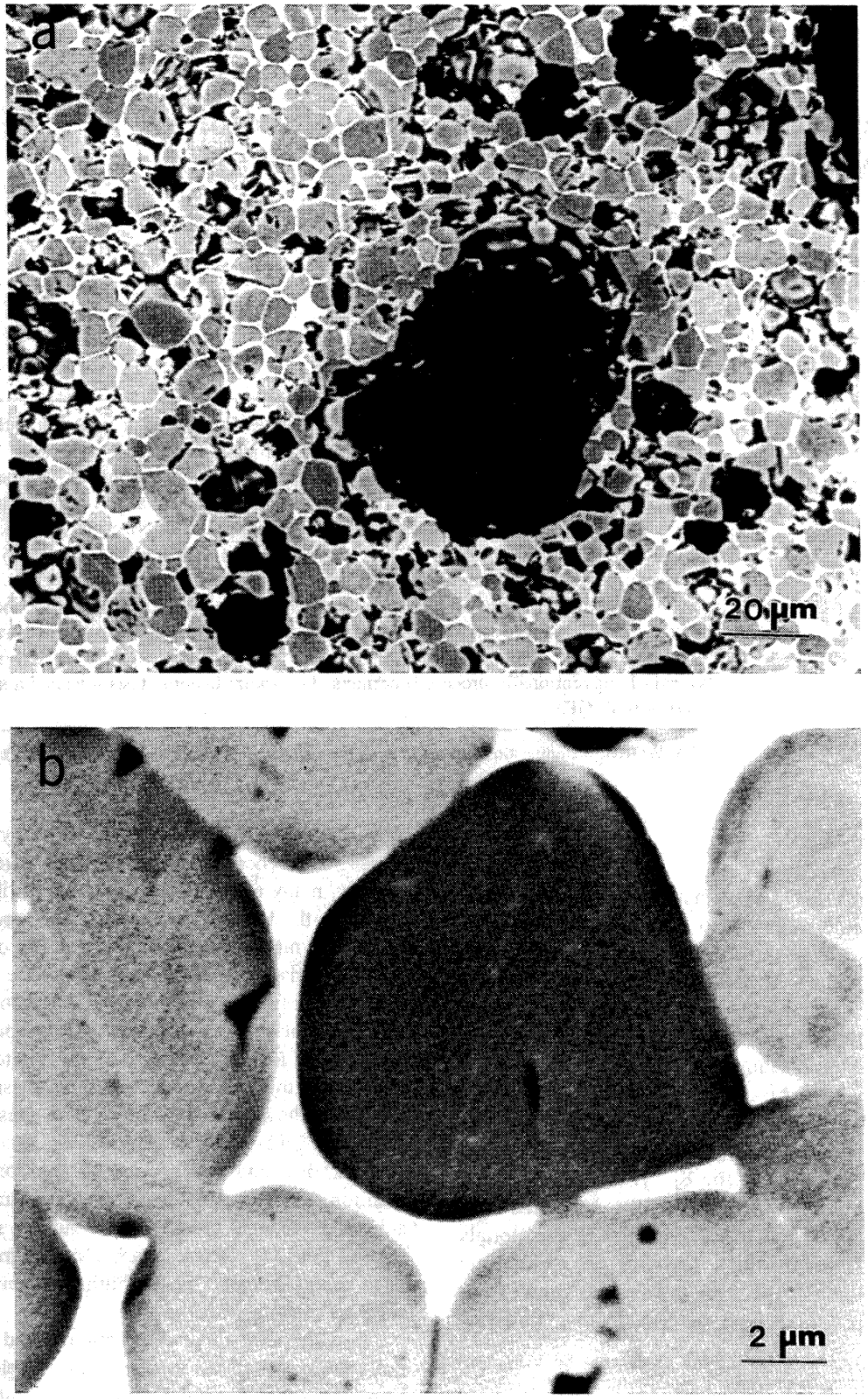

Fig. 1. Backscattered electron micrographs of (a) as-reacted TiC–25Ni and (b) sintering necks between TiC particles result in a rigid TiC skeletal structure.

cessfully used by the authors and co-workers [38, 39] to produce dense TiC and TiB_2 disks. Figure 1a shows the microstructure of the as-reacted TiC–25% Ni; the porosity (dark regions) exceeds 50%. Previous work by the authors and co-workers [38, 39] demonstrated that high-speed forging could reduce the porosity of as-synthesized TiC and TiB_2 to less than 5%. Figure 1b shows sintering necks between the spheroidal TiC particles which lead to a structure with a high stiffness. The main difficulty encountered in the densification of TiC was macrocracking, probably due to residual thermal stresses. The addition of a ductile phase should enhance the fracture toughness of the material, as well as providing relief for any residual stress. The objective of this paper is to show that dense TiC—Ni cermets can be produced by combining combustion synthesis with impact forging.

2. EXPERIMENTAL

High-purity (>99%) powders of elemental Ti (Micron Metals Inc., Salt Lake City, UT), C (Consolidated Astronautics, Smithtown, NY), and Ni (Aldrich Chemical Co., Milwaukee, WI) were used in this investigation. The particle sizes for the Ti, C, and Ni were 44 (−325 mesh), 2, and 3 μm, respectively. Ni additions of 5, 25, and 30 wt% were made to the Ti + C reaction. The 5 wt% Ni addition was chosen to minimize the effect on the mechanical properties; its function was to act as a sintering aid, as well as an internal stress reliever. The larger Ni additions were intended to enhance the fracture toughness of the product; for cutting tool applications a lower Ni content is preferred: ~10–20 wt% [7]. The theoretical product compositions fall into the two-phase γ (Ni solid solution) + δ (TiC) region of the quasi-binary TiC—Ni phase diagram as determined by Stover and Wulff [40].

Powders were dry-mixed in a ceramic grinding jar under an argon atmosphere for approximately 24 h. Ceramic grinding balls were added at 2:1 weight ratio to increase powder homogeneity and reduce the size of C agglomerates; these C agglomerates (~1 mm in size) can be sources of macrocracks. After mixing, the powders were removed from the ceramic grinding jar and placed within a vacuum oven for a minimum of 24 h to remove any absorbed water.

Powder compacts of cylindrical plate geometry were then produced using a steel die and axial stress of approximately 55 MPa (this stress corresponded to a powder compact density of approximately 65% of theoretical). The powder compacts for the 5 and 25 wt% compositions were approximately 9 cm in diameter and 400 g in mass. The powder compacts for the 30 wt% Ni were 6.35 cm in diameter and 200 g in mass.

During the combustion synthesis/dynamic densification process, the powder compacts were contained in two types of fixtures which are shown schematically in Fig. 2. These fixtures are designed such that they can confine the material during reaction and densification, allow the expulsion of volatile impurity gases evolved during the reaction, and provide thermal protection for both the material (thermal shock) and surrounding die. The basic components of the fixture used for the TiC + 5 wt% Ni and TiC + 25 wt% Ni compacts consisted of a tapered steel ring and refractory insulation sheets (Zircar Products, Inc., Florida, NY) which are bonded to the inner radius with alumina-based cement (Fig. 2a). For the TiC + 30 wt% Ni cermets, sand (−325 mesh) was added to improve material containment and near-net shaping; see Fig. 2b. This modification was made because of the large amounts of liquid phase present within the reacted compacts. During densification, the compact behaves as a porous viscous body; thus, containment becomes a problem which is solved by the use of the sand. The sand acts as a pressure transmitting medium, creating a macroscopic quasi-isostatic state of stress on the compacts (there does exist a small shear

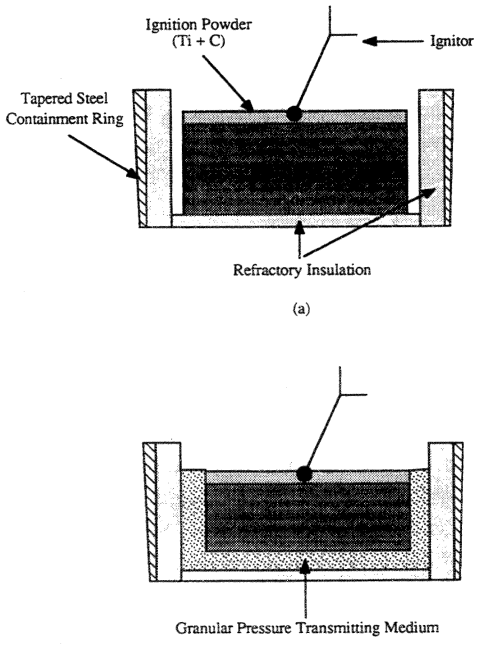

Fig. 2. Schematic representation of the hot-matter containment fixtures used in this study: (a) rigid fixture, TiC–5Ni and TiC–25Ni; and (b) modified fixture utilizing granulated pressure transmitting medium, TiC–30Ni.

stress component at the surface of the compact) [41, 42]. This approach was originally developed by researchers at the Institute for Structural Macrokinetics, Chernogolovka, Russia [41, 42]. In the United States, the use of the pressure transmitting granular medium is known as the CERACON process and has been applied to the densification of combustion synthesized materials by Raman *et al.* [26].

The technique used to initiate the propagation of the thermochemical reaction wave through the powder compacts consisted of placing 20 g of uncompacted Ti + C reactant powder on its top surface and then using an electric "match" to ignite the loose powder. This electric "match" consisted of Ni—Cr wire wrapped around a wooden match stick head. This electric match proved to be an improvement over the electric ignitor used in previous studies [38, 39].

It has been recognized in previous studies on the densification of combustion synthesized materials that there is a time "window" in which successful densification may be accomplished [11, 43]. In the study on the densification of combustion synthesized TiC [38], this window corresponded to the time between when the reaction was completed and when the temperature of the compact fell below the ductile-to-brittle transition temperature and was approximately 5–10 s after ignition. In the present work, tests were conducted with time delays of 10, 15, and 20 s. The time delay is measured from the moment of initiation of the ignition powder. Successful densification was achieved by both the 10- and the 15-s time delays, while the 20-s time delay resulted in a highly skeletal structure compact (it was fully dense). The cracks are attributed to the formation of the rigid skeletal structure before densification, thereby reducing the fracture toughness of the compact; Fig. 1b shows the profuse sintering necks between the TiC particles, which lead to a skeletal structure that is characteristic of the as-synthesized TiC—Ni.

Densification was accomplished utilizing the Dynapak high-speed forging machine (10–15 m/s). Figure 3 is a schematic illustration of the machine showing some of its pertinent features. Details of this machine are contained elsewhere [45]. Once the time "window" for successful densification was determined and the powder compacts were loaded into the hot-matter containment fixture, this assembly was placed within the cylindrical cavity of the bottom die. The ignition powder (i.e., uncompacted Ti + C) was then placed on top of the compact, followed by placement of the electric match into this powder. This match was then ignited remotely, and after the predetermined time delay, the hammer was released, densifying the hot compact. Densified compacts were placed in sand or vermiculite for slow cooling. Periodic inspection using a thermocouple revealed that the temperature after 12 h was above 200°C.

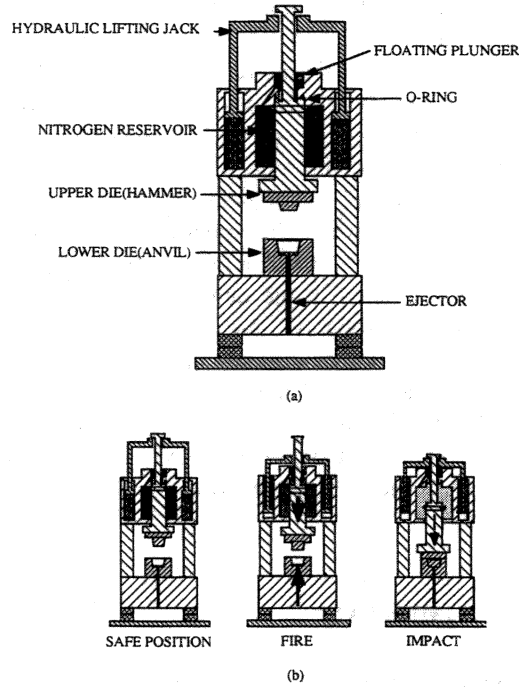

Fig. 3. Schematic of high-velocity forging machine: (a) machine components; (b) operation sequence.

The compacts were then sectioned for metallographic (apparent density and grain size measurements), X-ray diffraction, scanning electron microscopy, and Vickers microhardness analysis. Transmission electron microscopy was conducted on the TiC–25Ni and TiC–30Ni materials. During metallographic preparation, specimens were final polished using 0.05-μm colloidal silica after 0.25-μm diamond paste. X-Ray diffraction analysis was conducted using a Philips Model PW 1729 X-ray generator (CuKα) and a PW 1840 diffractometer. The Cambridge Stereoscan 360 scanning electron microscope (20-kV accelerating voltage) was used to examine general microstructural features, while qualitative elemental analysis was performed with the Link Analytical AN1085 system using a Be window detector. To increase the resolution of the elemental analysis, an accelerating voltage of 10 kV was used. Transmission electron microscopy was conducted on both the TiC–25Ni and the TiC–30Ni materials using a Philips CM30 electron microscope. Conventional TEM imaging and diffraction were conducted at 300 kV. Finally, microhardness measurements were conducted at room temperature using a Leco Model M-400 Hardness Tester

with a Vickers diamond indentor and a 500-gf load. Mean microhardness values and standard deviations correspond to 100 measurements. Quasi-static mechanical tests were performed in an Instron machine, using specimens with 4 × 4 × 7-mm dimensions for compression tests which were cut by electric discharge machining. The variation in specimen length was less than 5 μm (flatness). Stainless-steel shims (2.5-μm thickness) were used to eliminate loading inhomogeneities. Four-point bending tests were conducted using specimens with 4 × 4 × 30-mm dimensions.

3. RESULTS AND DISCUSSION

3.1. X-Ray Diffraction

X-Ray diffraction results for the as-reacted material are shown in Fig. 4. For comparison, the X-ray diffraction spectrum for the initial reactant mixture is also shown. As can be seen, the final product contains both TiC and Ni peaks; TiC and Ni are thermodynamically stable phases [40]. It has been reported that compounds in the Ti—Ni system form during the combustion reaction in the Ti—C—Ni system. Wong *et al.* [46], using time-resolved X-ray diffraction on a Ti—C–25Ni reactant mixture, showed that a Ni—Ti compound formed before TiC. The intensity of its peaks decreased with time but did not completely disappear and therefore it was found in the final product (Ni_3Ti or NiTi). In another study, Henshaw *et al.* [47] observed the propagation of two combustion waves during the combustion synthesis of a Ti—C—20Ni reactant mixture. The intensity of the first wave was observed to be rather weak, while that of the second wave was strong. Quenching of the reaction after the first combustion wave and using X-ray diffraction analysis after passage of the second combustion wave revealed the products to consist mainly of TiC and Ni, with some residual C and very small amounts of the Ni—Ti compounds. The propagation of two distinct combustion waves was observed for the Ti—C—25Ni reactant mixture used in this study; however, the initial combustion wave typically propagates in the spin mode and is overtaken quickly by the second more intense combustion wave (planar mode) before it has the opportunity to propagate extensively into the specimen. Thus, one expects that the propagation of the first combustion wave depends strongly on the conditions of the ignition and heat loss since under different experimental conditions the propagation of the first combustion wave can be transient (our observations) or stable [47]. This is not at all surprising since this has been shown both experimentally and theoretically in the field of combustion [48]. However, in this study, no Ni—Ti compounds were detected using X-ray diffraction analysis. On the other hand, a small amount of C appears to be in the final product. This could be due to incomplete combustion caused by heat losses or due to titanium dissolving in nickel, creating a carbon excess. In addition, in studies on the combustion synthesis in the Ti—C system, it was shown that C is lost due to its interaction with the oxide scale covering the Ti particles [49, 50].

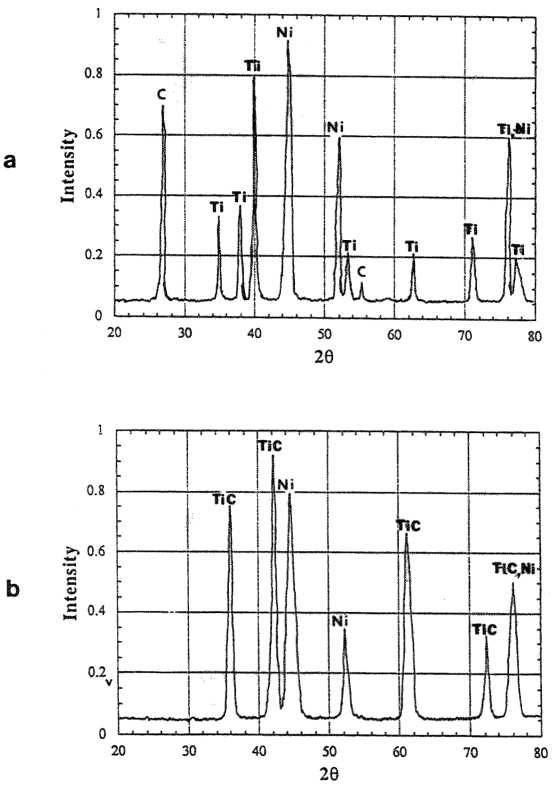

Fig. 4. X-ray diffraction spectrum of the (a) initial reactants and (b) as-reacted material showing both TiC and Ni peaks.

3.2. Microstructural Characterization

The microstructure of the synthesized and densified TiC–5Ni is shown in Fig. 5a. As can be seen, the microstructure consists of spheroidal TiC grains, with a discontinuous Ni layer located at the boundaries and triple points. The Ni is discontinuous because, when in the liquid state, it does not completely wet TiC [51]. Thus, interfaces between TiC grains are thermodynamically favorable. It is interesting to see the many voids within the TiC—5Ni material. The conditions of the combustion synthesis/dynamic densification process

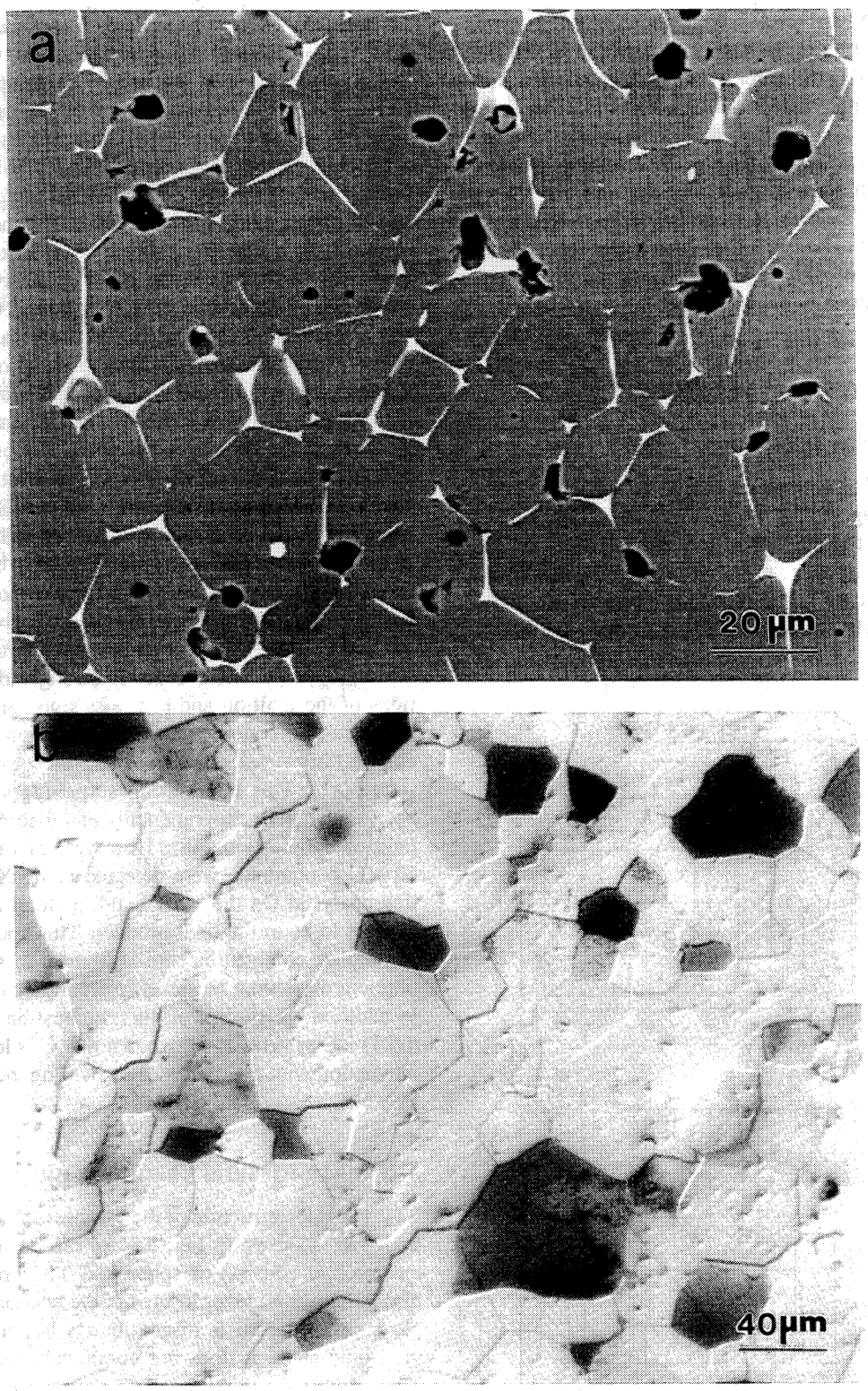

Fig. 5. Combustion synthesized/dynamically densified (a) TiC–5Ni material (backscattered electron micrograph) and (b) TiC (optical micrograph).

were the same as for the material shown in Fig. 5b, which shows densified TiC without Ni addition; only minor porosity is seen in the latter case. It was expected that densification would be easier with the presence of a small amount of Ni since it was thought to be liquid at the combustion temperatures. In previous experiments without densification, it was observed that during the reaction, the compact would partially blow apart. Ni vaporizes at approximately 2,884°C [52]; adiabatic temperature calculations predict that 70% of the Ni vaporizes. During densification, if some of the Ni vapor is still being evolved, it could provide an increase in the resistance to densification by generating a back-pressure within the collapsing skeletal structure.

Figure 6 shows the resulting microstructure for the TiC–25Ni material. As can be seen, it consists of a spheroidal TiC phase embedded in a nearly continuous Ni binder. The morphology of the TiC phase is interesting because particles exhibit multiple cusps which seem to indicate that they actually consist of agglomerates of smaller grains. This is shown clearly in Figs. 6a and b. Another interesting feature seen in Figs. 6a and b is the appearance of TiC grains impinging upon one another with a thin layer of Ni trapped between them. Comparison with the microstructure of the as-reacted TiC–25Ni material shown in Fig. 1b shows the effect that the densification step can have on the resulting microstructure. The increased Ni content reduces the energy required for densification. As a result, the compact extruded out from under the hammer. The material that remained underneath the hammer was only 2 mm thick. The probable explanation for the multiple cusps exhibited by some of the TiC phase is that during densification, the small TiC grains agglomerated under the action of the applied load. Because most of the material was extruded from underneath the hammer, the material remaining underneath the hammer was effectively quenched. If the temperature was able to remain above the melting point of Ni for some time, these cusps would disappear because they represent a higher energy state and would therefore preferentially (solubility within the liquid is inversely proportional to the radii of the cusps) so into solution and later reprecipitate onto the larger grains or particles. A separate report is being prepared on the micromechanisms of reaction synthesis [53]. Based upon this result, modification of the hot-matter containment fixture was necessary. The importance of Ni being in the liquid phase during densification is not only in the ease of densification, but also in the microstructural evolution of the material.

In comparison to the microstructure for the TiC–25Ni material, the TiC phase in the TiC–30Ni material does not exhibit the multiple cusps as can be seen in Fig. 7. The use of the pressure transmitting medium greatly enhanced material confinement. The microstructure consists of spheroidal TiC grains embedded in a nearly continuous Ni binder. The particle sizes for the TiC phase, as determined by the linear intercept method, are approximately 8 and 5 μm for the TiC–25% Ni and TiC–30% Ni, respectively. The TiC phase does appear to exhibit a small degree of faceting. In addition, because Ni does not completely wet TiC, the TiC grains form a continuous carbide skeleton. Given the apparent size of the TiC particles, it is possible that due to the high temperature reached during the combustion reaction, the microstructure is typified as one that has been coarsened by a dissolution–reprecipitation process. This dissolution–reprecipitation process is also responsible for grain coarsening during liquid-phase sintering [54].

3.3. Transmission Electron Microscopy

Detailed substructure features of the TiC and Ni phases, as well as their interfaces were revealed by transmission electron microscopy (TEM). Figure 8 shows a spherical TiC particle (monocrystalline) surrounded by other TiC grains and Ni binder in the TiC–25Ni material. The beam direction of the selection area diffraction pattern is [011]. The cubic structure of TiC is confirmed. The particles contain one or a few grains. Dislocation arrays (or cells) are prominent in the TiC grains. Figure 9 shows one such dislocation array (or cell) within a TiC grain. Based upon the studies by Hollox and Smallman [55] and Das *et al.* [56], these dislocation substructures are characteristic of an annealed microstructure. It is believed that these dislocation arrays (or cells) were formed during the densification step. Densification occurred primarily by deformation of the nickel; the TiC particles would be distorted into prolate spheroids if they had undergone plastic deformation. Clearly this is not the case. The recrystallization temperature for nickel ($\sim T_m/2$) is approximately 600°C. Independent thermocouple experiments indicate that densification takes place at approximately 1700°C. Thus, the temperature difference is amply sufficient to ensure recrystallization and grain growth in the nickel phase, eliminating any effects of plastic deformation. In some TiC grains, these dislocation arrays (or cells) have arranged themselves into subgrains with low angle grain boundaries. Figure 10 shows the interface between a large TiC grain (which exhibited the cusp morphology) and a small TiC grain which makes up part of the cusp.

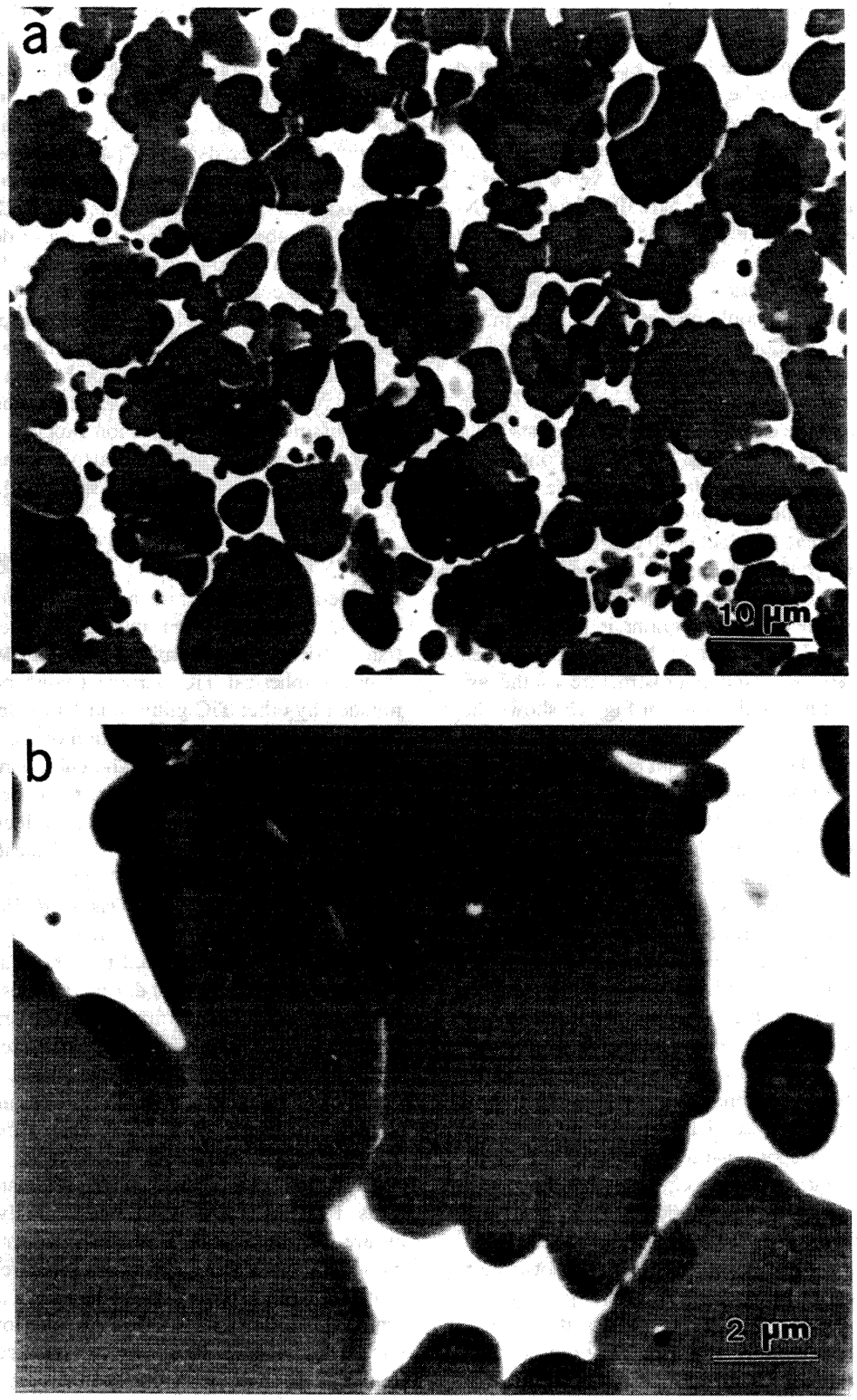

Fig. 6 Backscattered electron micrographs of the combustion synthesized/dynamically densified TiC–25Ni material: (a) spheroidal TiC phase embedded in a nearly continuous Ni-alloy binder, and (b) TiC phase exhibiting multiple cusps.

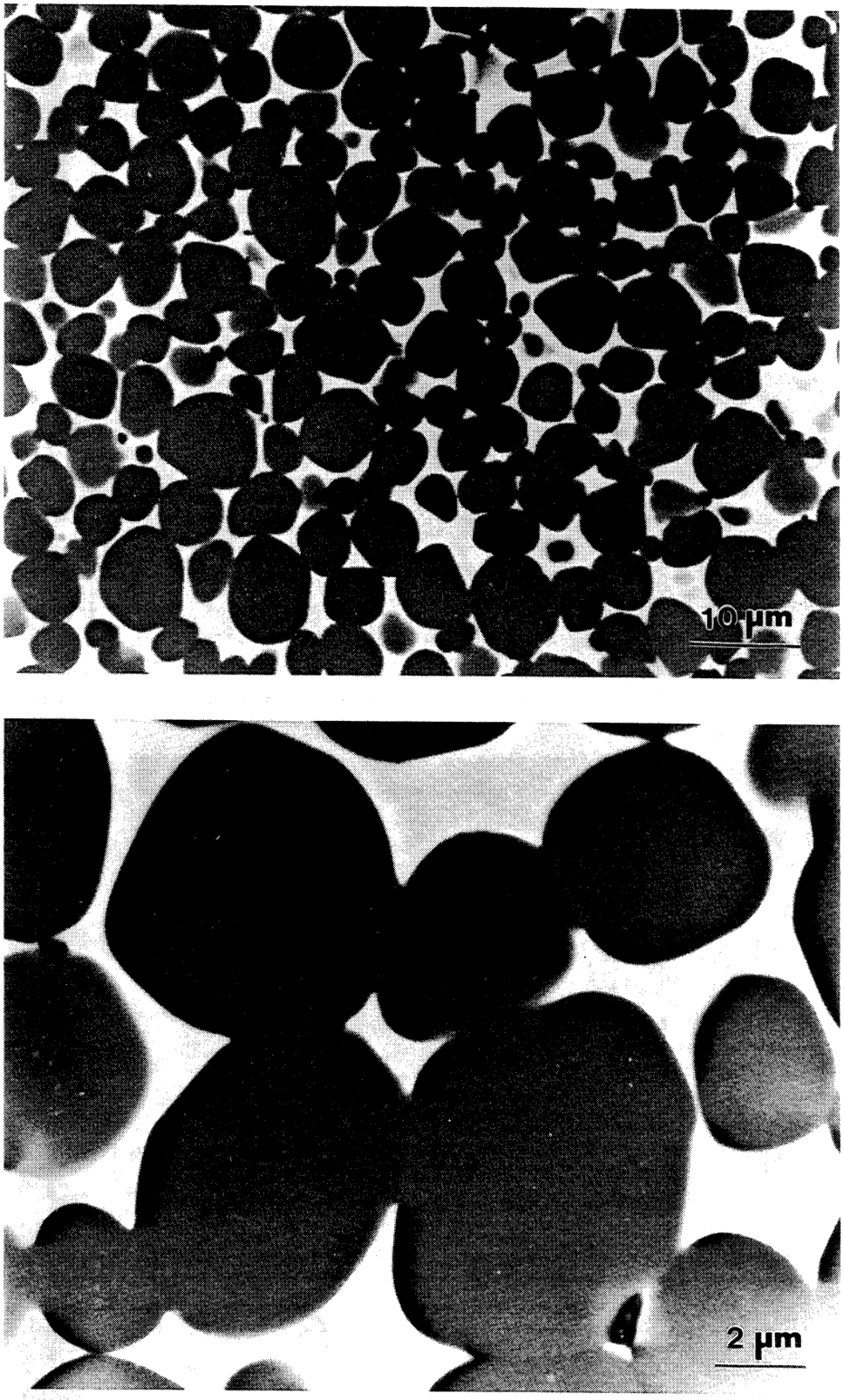

Fig. 7. Backscattered electron micrographs of the combustion synthesized/dynamically densified TiC–30Ni material: (a) spheroidal (with some faceting) TiC phase embedded in a nearly continuous Ni–alloy binder and (b) sintering necks between TiC particles.

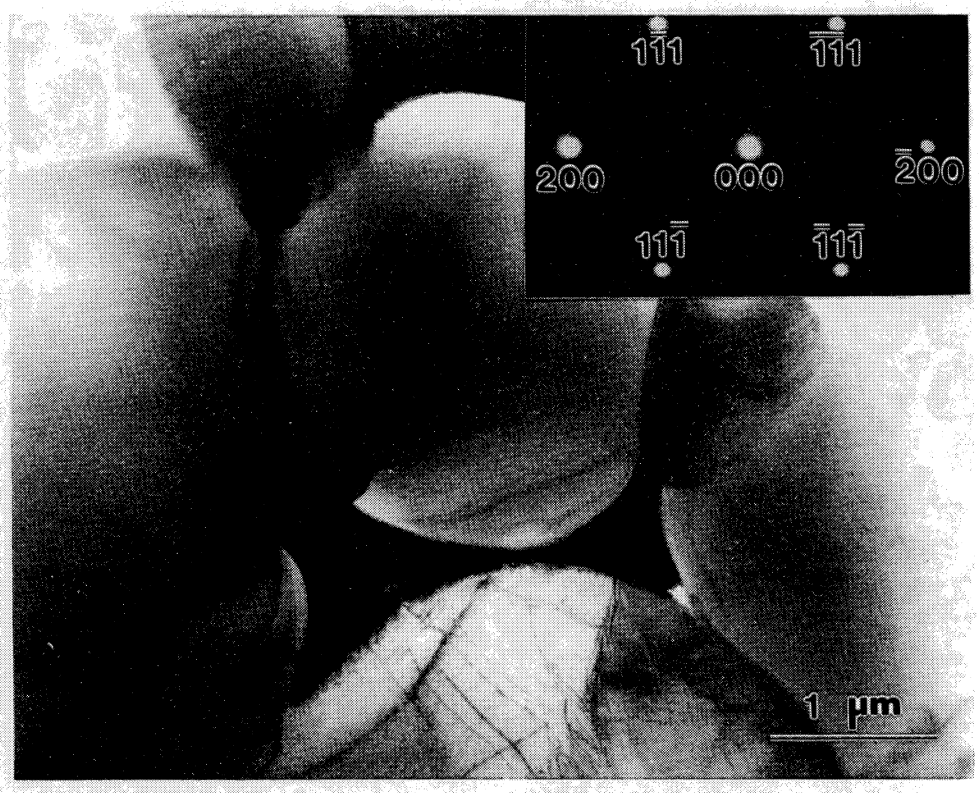

Fig. 8. Transmission electron micrograph of the TiC phase in TiC–25Ni material and selected area diffraction pattern.

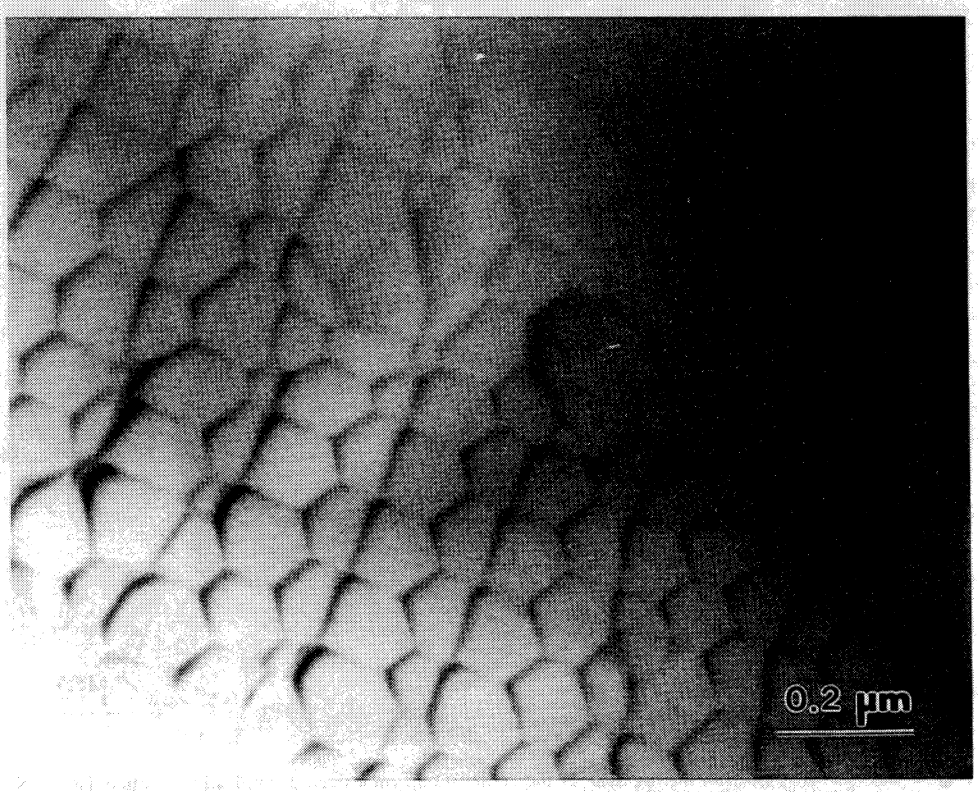

Fig. 9. Dislocation array within a TiC grain (TEM).

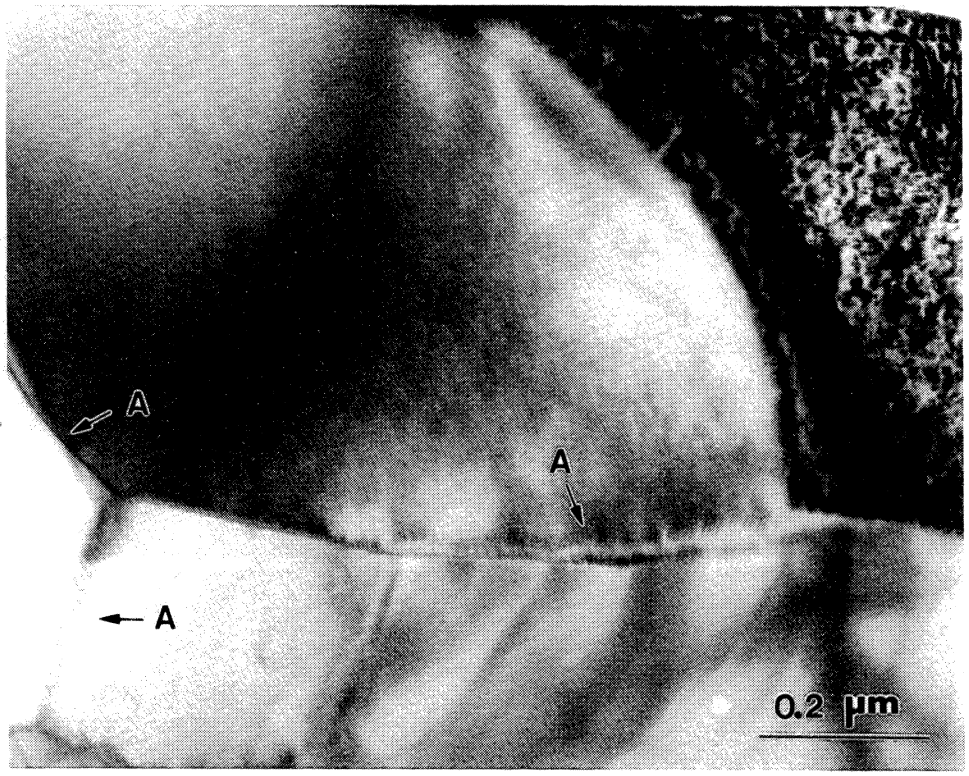

Fig. 10. Grain boundary within the TiC phase of the TiC–25Ni material. Other grain boundaries are also seen (arrows) (TEM).

As can be seen, this interface is composed of dislocations (arrows A).

Most of the TiC—TiC interfaces were free of any potentially harmful second phase or contaminations. Figure 11 shows an interface between two TiC particles in which a sintering neck was formed. Small lens-shaped pockets of a second phase can be seen (marked by arrows). Using energy-dispersive x-ray microanalysis (EDXM), these particles were found to be Ni-rich. Titanium is undoubtedly also present in the Ni phase because of the solubility. One possible explanation for these particles is that, during densification, a thin Ni layer became trapped between the two TiC grains. Because Ni does not wet completely, the TiC and Ni layer separate into several small particles (interfacial energy minimization). Confirmation of this can be seen in Fig. 6, in which a thin Ni layer appears to be trapped within the TiC grain.

The dislocation substructures in the TiC–30Ni material were also characterized as being those typical of an annealed microstructure. Figure 12 clearly shows the faceting of the TiC grains. Figure 13 shows a monocrystalline TiC particle which contains relatively few dislocations. On the other hand, Fig. 14 shows the interface region between two TiC grains, which is so heavily dislocated that recrystallization cells have formed in each grain (marked A and B, respectively). Figure 14b is a closeup of this region. Figure 15 shows another neck region between two TiC grains which are heavily dislocated. It is believed that these dislocation arrays were formed during densification by the impingement between TiC particles.

The Ni phase in the TiC–25Ni material consists of large grains which are virtually devoid of dislocations. The Ni melts and, prior to or after densification, solidifies and/or recrystallizes around the TiC particles. The dislocations shown in Fig. 16 were probably introduced during cooling due to a mismatch in the thermal expansion coefficient of Ni and TiC. Using EDXM, the Ni binder was found to contain a considerable amount of Ti in solution. This is not surprising since it was mentioned earlier that TiC is soluble in Ni. The Ni phase was again devoid of dislocations. Some Ni grains exhibited low-energy boundaries (probably coherent annealing twin boundaries) as shown in Fig. 17. The length of this boundary is not minimized and it is very straight;

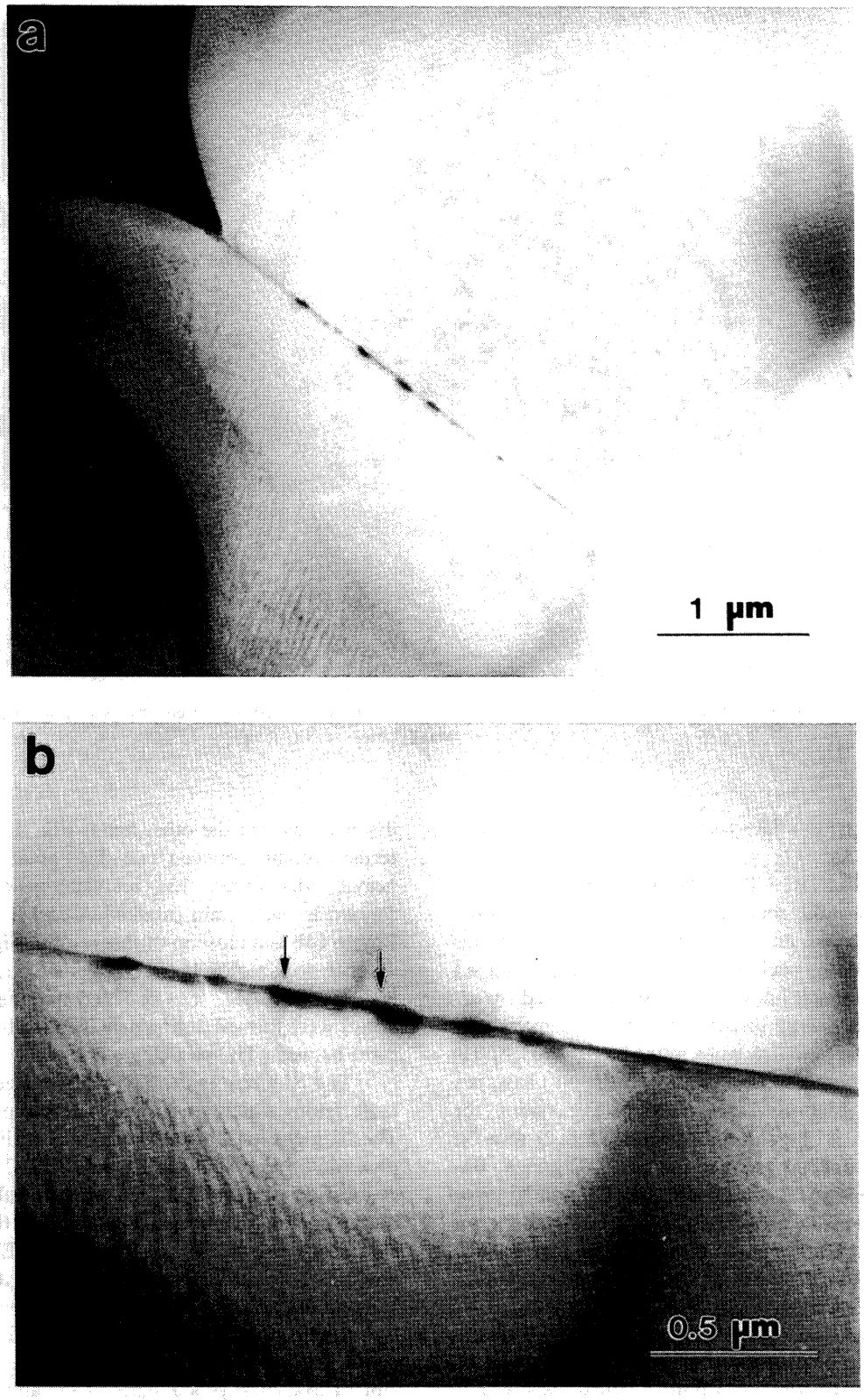

Fig. 11. (a) Sintering neck between two TiC grains; (b) note the presence of small Ni-rich second-phase particles at the interface (arrow) (TEM).

Fig. 12. Faceting of the TiC phase within the TiC–30Ni material (TEM).

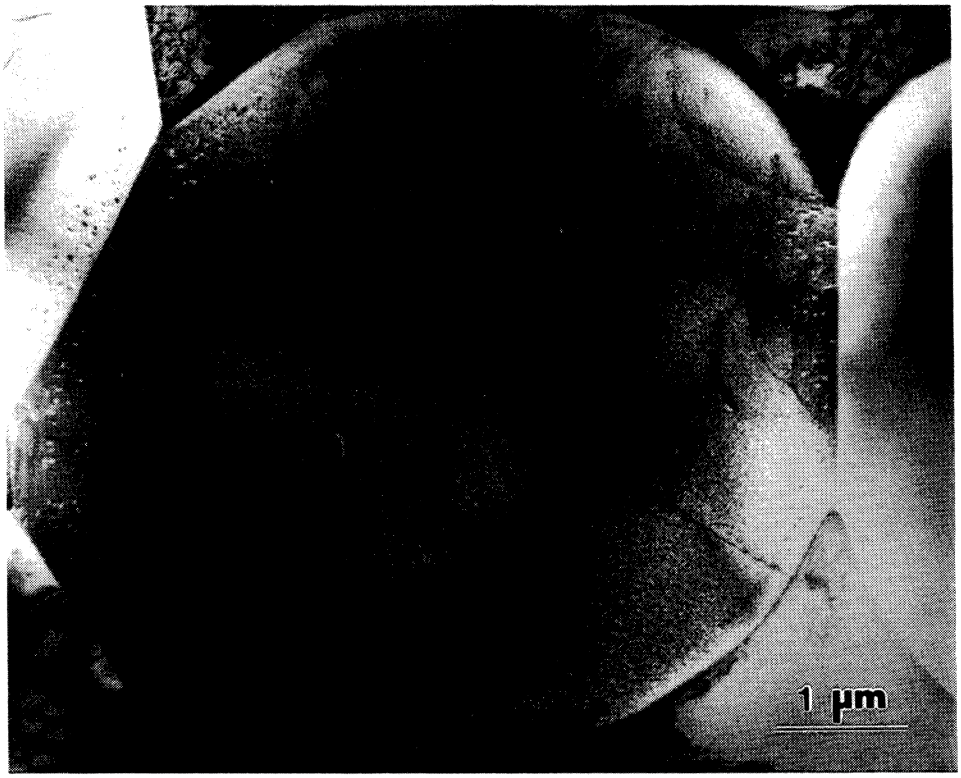

Fig. 13. Low dislocation density within a TiC grain (TEM).

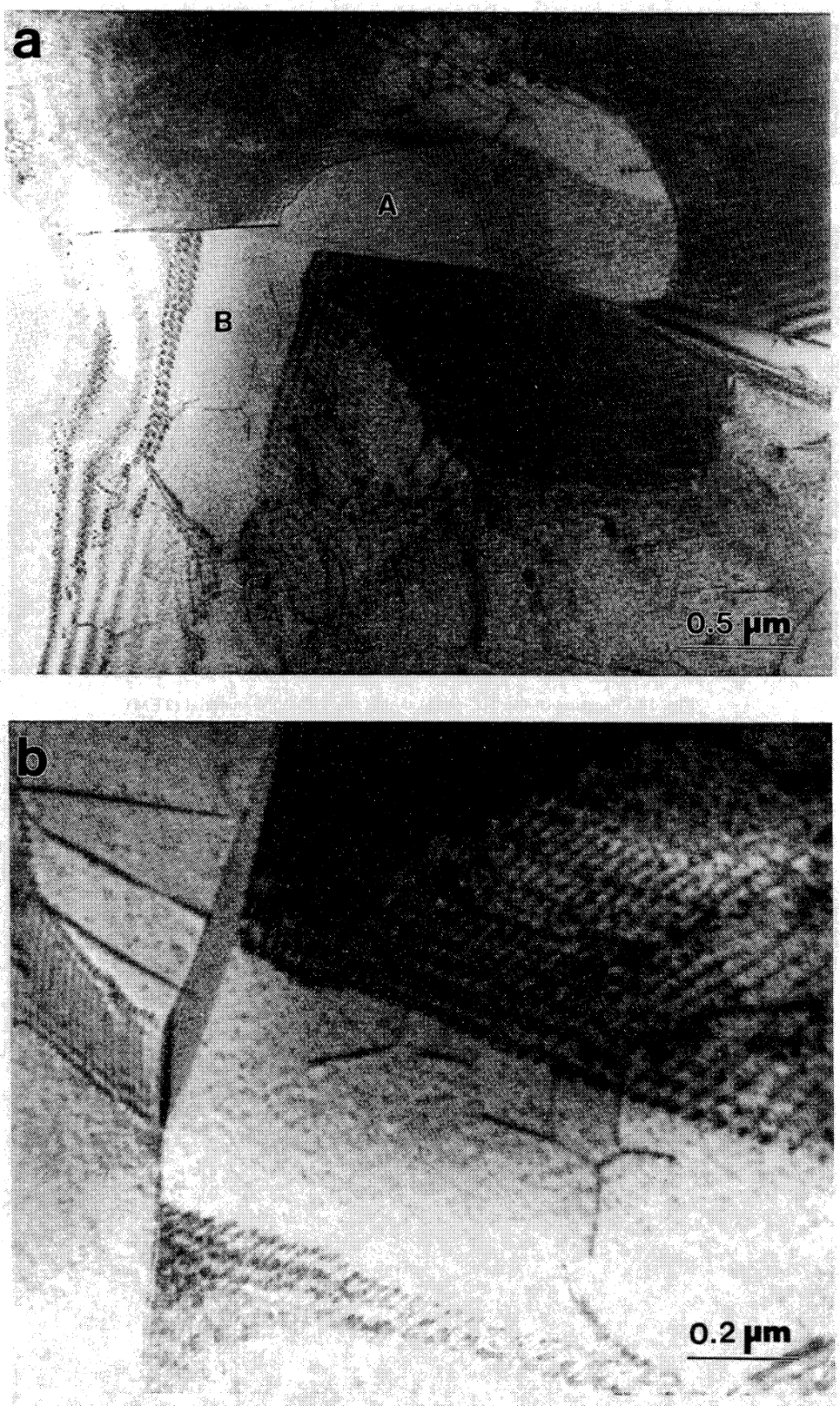

Fig. 14. High dislocation density at the interface between two TiC grains. Note the formation of recrystallization cells (TEM). (a) Lower magnification; (b) higher magnification.

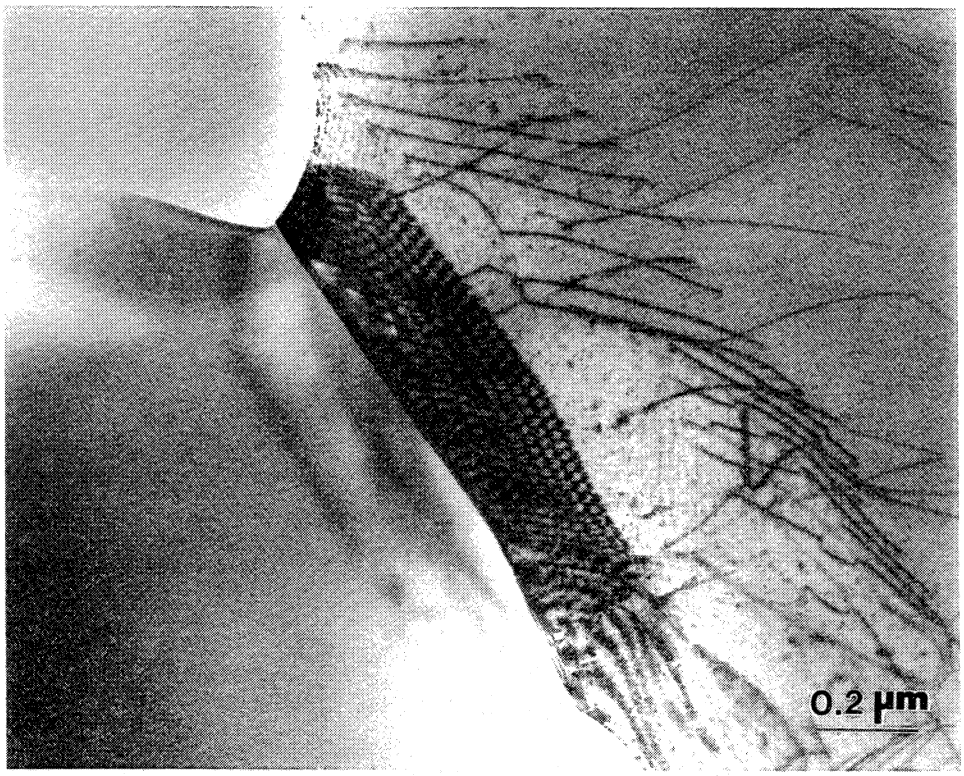

Fig. 15. Neck region between the two TiC grains showing dislocation array (TEM).

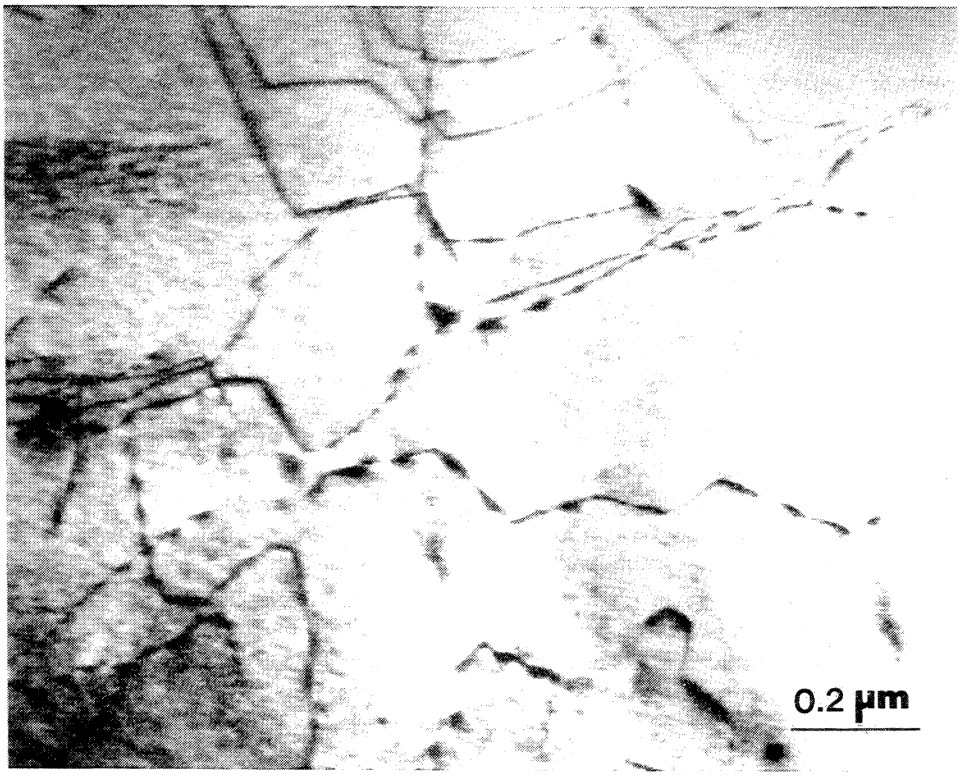

Fig. 16. Dislocations within the Ni Phase (TEM).

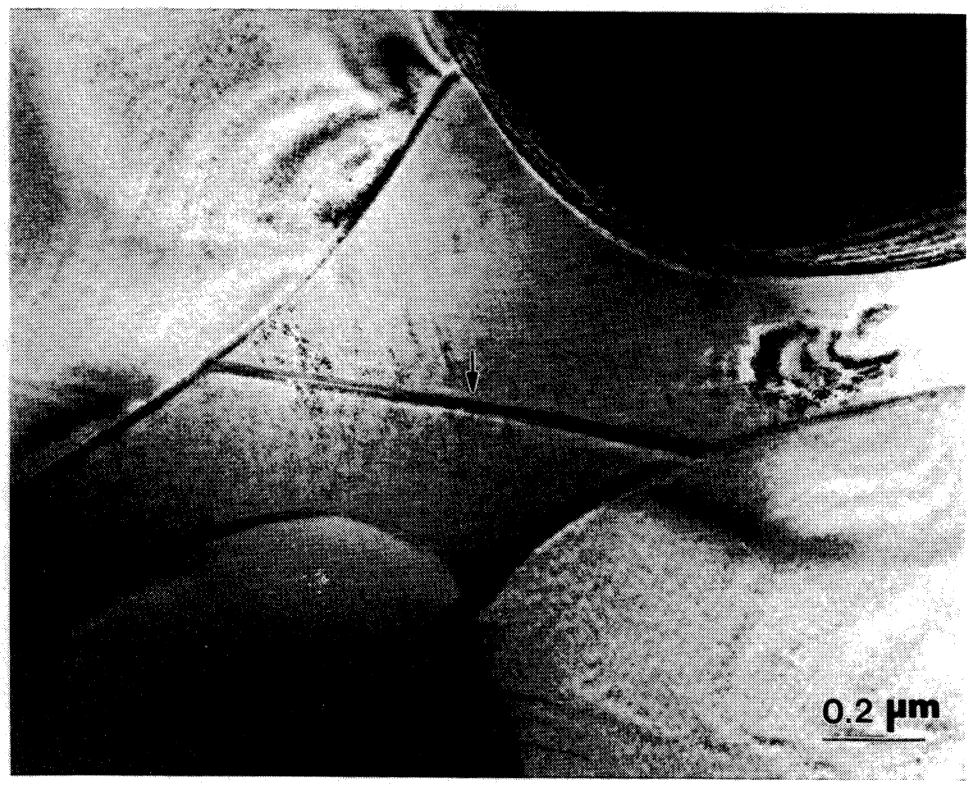

Fig. 17. Annealing twin or stacking fault within the Ni phase (TEM).

both factors support the contention that the energy is at the bottom of a cusp. The interface between the TiC grains and the Ni phase appeared to be free of potentially detrimental second phase particles. Dislocations within the TiC grains appear to impinge upon the interface with Ni.

3.3. Mechanical Properties

Compression testing of Ti–30Ni specimens was carried out at a strain rate of 10^{-3} s^{-1}. The failure occurred without appreciable plastic deformation. Three tests were carried out, yielding an average strength of 2.9 GPa. Failure took place by a mixed shear-axial splitting mode, with shear being confined to the regions adjoining the compression platens. Figure 18 shows scanning electron micrographs of the failure regions. In the tensile (axial splitting) failure region ductile necking of the Ni phase, leading to knife-edge cusps, is shown by arrows in Fig. 18a. Failure of the TiC particles occurred by brittle cracking, and no evidence of TiC—Ni separation is seen. This is in line with TEM results, which show that the TiC—Ni interface is clean. In the shear failure region (Fig. 18b), rubbing of the failure surfaces led to comminution of the particles, and they mask the fracture surfaces.

The microhardness for the TiC–30Ni specimen was 13.1 ± 1.6 GPa; this value is in the range of values for conventionally processed cermets of similar composition [7].

Three four-point bend tests were conducted, yielding an average transverse rupture strength of 0.47 GPa. This value is a considerable improvement over the transverse rupture strength of TiC (with no Ni additions). The increased tensile strength is due to the effective crack-arrest ability of the nickel. Figure 19 shows incipient failures in the specimens. Regions with residual porosity were responsible for the initiation of cracking, as seen in Fig. 19a. Figure 19b shows that the crack propagated in both phases and that the existence of two phases was an effective crack arrester.

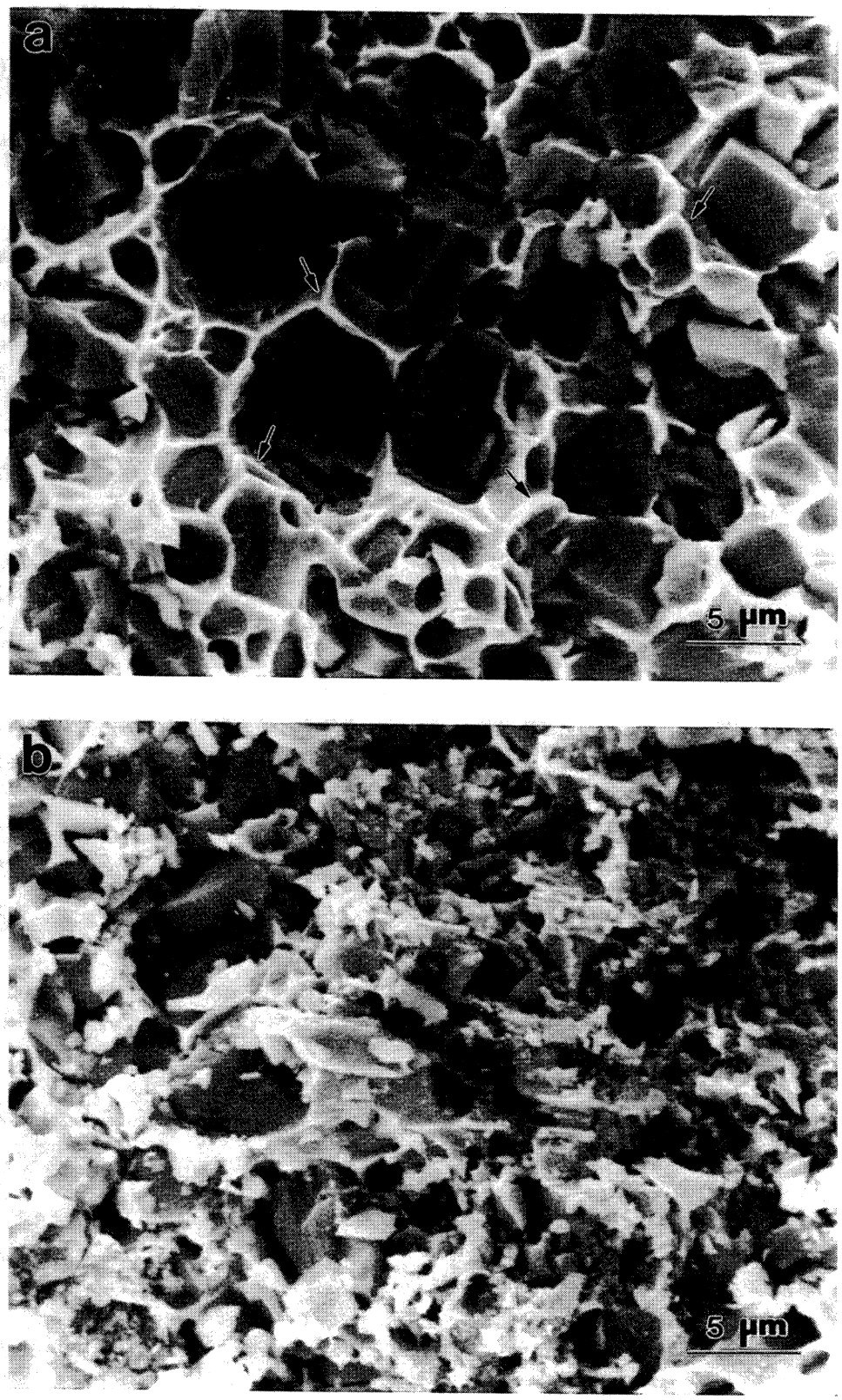

Fig. 18. Scanning electron micrographs of TiC–30Ni fractured in compression test: (a) axial splitting region and (b) shear failure region.

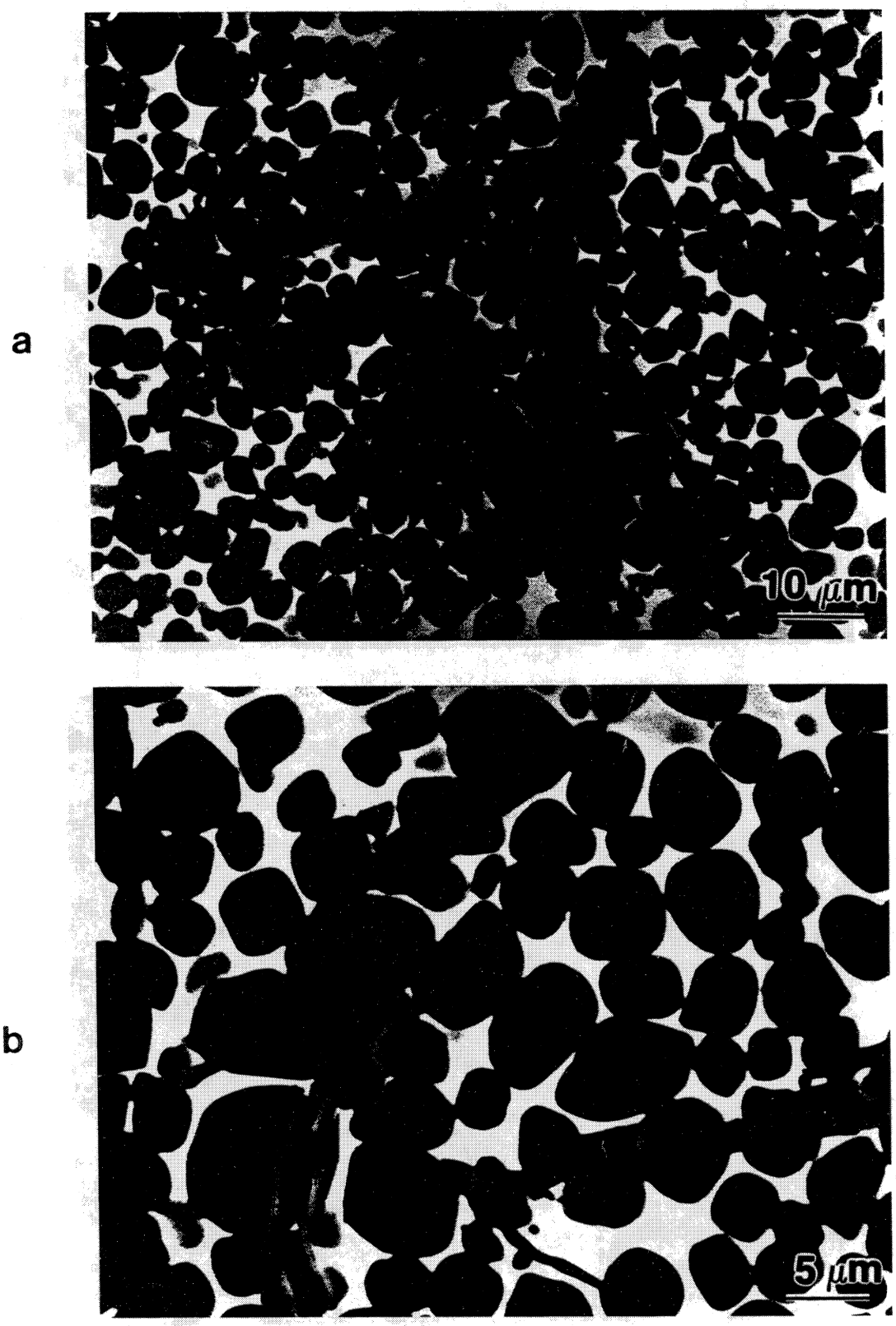

Fig. 19. (a) Residual porosity in the TiC–30Ni material which gives rise to crack formation in compression; (b) typical crack propagation path.

4. CONCLUSIONS

Dense TiC—Ni cermets with Ni contents of 5, 25, and 30 wt% were produced by combining combustion synthesis with impact forging. The microstructures consisted of spheroidal (with some faceting) TiC grains separated by a discontinuous Ni layer.

The porosity in the TiC–5Ni material may be due to the partial vaporization of the Ni. Adiabatic temperature calculations predict that 70% of the Ni would be vaporized during synthesis and that the addition of 8 wt% Ni would eliminate the vaporization of Ni. Thus, for low Ni contents (2–3%), dilution of the reaction using presynthesized TiC would be required. The addition of small amounts of Ni is attractive since it reduces the forces necessary for densification without much detrimental effect to the mechanical properties.

The microstructure of the TiC–25Ni material was characterized by nonequilibrium morphologies (i.e., multiple cusps) of the TiC phase. Transmission electron microscopy revealed that some TiC particles were polycrystalline. The presence of multiple cusps in some TiC particles is believed to be the result of lack of proper containment during densification. This led to the use of the pressure-transmitting granulated medium for the TiC–30Ni material, which allowed a near-net shape capability.

The microstructure of the TiC–30Ni material was characterized by spheroidal TiC particles surrounded by Ni; a substantial fraction of the TiC particles exhibited bonding and necking. The apparent mean size of the TiC particles was approximately 5 μm; it is believed that the TiC particles have undergone coarsening by the dissolution–reprecipitation process common in liquid-phase sintering. The low density of dislocations in both the TiC and the Ni phases is evidence that recrystallization occurred after the plastic deformation associated with densification. The isotropy of the microstructure confirms this evidence and indicates that is formed after plastic deformation.

Hardness and compressive mechanical tests indicate that the properties of the reaction synthesized/dynamically densified material are within the range of conventionally processed cermets and that the bonding between Ni and TiC is excellent.

ACKNOWLEDGMENTS

This research was supported by the U.S. Army Research Office under Contracts ARO-DAAL-03-88-K-0194 and ARO-DAAL-03-90-G-0204 and by the National Science Foundation under Grant CBT 8713258; we thank Dr. E. Chen for the continuing support and encouragement. Mr. J. LaSalvia was supported by a fellowship under the URI Program on Ultradynamic Performance Materials for 1992–1993. Discussions with Dr. R. V. Raman, A. Niiler, and Mr. Rele are gratefully acknowledged. Help provided by Dr. B. Kad in electron microscopy is greatly appreciated.

REFERENCES

1. G. T. Dzodziev, A. A. Kal'kov, A. A. Dubrovskii, V. A. Gotlib, E. F. Korzukhina, and T. A. Shapoval, *Sov. Powder Metall. Met. Ceram.* **144**(4), 318–320 (1983).
2. V. A. Zhilyaev, E. I. Patrakov, and G. P. Shveikin, in *Proceedings of the International Conference on the Science of Hard Materials held September 23–28, 1984, Rhodes, Science of Hard Materials*, E. A. Almond, C. A. Brookes, and R. Warren, eds. (Institute of Physics Conference Series Number 75, Adam Hilger, Boston, 1986), pp. 1063–1073.
3. H. Doi, in *Proceedings of the International Conference on the Science of Hard Materials held September 23–28, 1984, Rhodes, Science of Hard Materials*, E. A. Almond, C. A. Brookes, and R. Warren, eds. (Institute of Physics Conference Series Number 75, Adam Hilger, Boston, 1986), pp. 489–523.
4. G. T. Fisher II, L. L. Oden, and G. Asai, *Bureau of Mines Report of Investigations*, RI 9115 (United States Department of the Interior, Washington, DC, 1987).
5. D. Moskowitz and M. Humenik Jr., in *Modern Developments in Powder Metallurgy*, H. H. Hausner, ed. (Plenum, New York, 1966), Vol. 3, pp. 83–94.
6. P. Schwarzkopf and R. Kieffer, *Cemented Carbides* (Macmillan, New York, 1960).
7. K. J. A. Brookes, *World Directory and Handbook of Hardmetals*, 2nd ed. (Engineers' Digest, London, 1979).
8. R. W. Stevenson, *Powder Metallurgy*, ASM Metals Handbook, 9th ed. (ASM, 1987), Vol. 7, pp. 773–783.
9. A. G. Merzhanov and I. P. Borovinskaya, *Dokl. Akad. Nauk. SSSR (Chem.)* **204**(2), 429 (1972).
10. N. P. Novikov, I. P. Borovinskaya, and A. G. Merzhanov in *Combustion Processes in Chemical Technology and Metallurgy*, A. G. Merzhanov, ed. (Chernogolovka, 1975) (English translation).
11. A. G. Merzhanov, in *Combustion and Plasma Synthesis of High Temperature Materials*, Z. A. Munir and J. B. Holt, eds. (VCH, New York, 1990), pp. 1–53.
12. J. F. Crider, *Ceram. Eng. Sci. Proc.* **3**, 519–528 (1982).
13. W. L. Frankhouser, K. W. Brendley, M. C. Kleszek, and S. T. Sullivan, *Gasless Combustion Synthesis of Refractory Compounds* (Noyes, NJ, 1985).
14. Z. A. Munir, *Am. Ceram. Soc. Bull.* **67**(2), 345 (1988).
15. Z. A. Munir and U. Anselmi-Tamburini, *Mater. Sci. Rep.* **3**, 277–365 (1989).
16. H. C. Yi and J. J. Moore, *J. Mater. Sci.* **25**, 1159 (1990).
17. J. B. Holt and Z. A. Munir, *J. Mater. Sci.* **21**, 251–259 (1986).
18. S. D. Dunmead, D. W. Readey, C. E. Semler, and J. B. Holt, *J. Am. Ceram. Soc.* **72**(12), 2318–2324 (1989).
19. Y. Miyamoto, M. Koizumi, and O. Yamada, *J. Am. Ceram. Soc.* **67**(11), C-224 (1984).
20. Y. Taneoka, O. Odawara, and Y. Kaieda, *J. Am. Ceram. Soc.* **72**(6), 1047–1049 (1989).
21. S. Adachi, T. Wada, T. Michara, Y. Miyamoto, and M. Koizumi, *J. Am. Ceram. Soc.* **73**(5), 1451–1452 (1990).
22. G. Y. Richardson, R. W. Rice, W. J. McDonough, J. M. Ku-

netz, and T. Schroeter, *Ceram. Eng. Sci. Proc.* **7**, 761–770 (1986).
23. M. A. Riley and A. Niiler, *Ballistics Research Laboratory Report*, BRL-MR-3574 (Aberdeen Proving Ground, MD, March 1987).
24. C. P. Cameron, J. H. Enloe, L. E. Dolhert, and R. W. Rice, *Ceram. Eng. Sci. Proc.* **11**(9–10), 1190–1202 (1990).
25. S. D. Dunmead, Z. A. Munir, J. B. Holt, and D. D. Kingman, *J. Mater. Sci.* **26**, 2410–2416 (1991).
26. R. V. Ramanj, S. V. Rele, and M. J. Paskowitz, *J. Metals* **45**(1), 54–55 (1993).
27. R. W. Rice, W. J. McDonough, G. Y. Richardson, J. M. Kunetz, and T. Schroeter, *Ceram. Eng. Sci. Proc.* **7**, 751–760 (1986).
28. KRI Kiser Research, Inc., Washington, DC 20036, Jan. (1989), pp. 1–11.
29. O. Yamada, Y. Miyamoto, and M. Koizumi, *J. Am. Ceram. Soc.* **70**(9), C-206–C-208 (1987).
30. S. Adachi, T. Wada, T. Mihara, Y. Miyamoto, M. Koizumi, and O. Yamada, *J. Am. Ceram. Soc.* **72**(5), 805–809 (1989).
31. J. B. Holt, G. M. Bianchini, and D. D. Kingman, UCRL-93467 (Lawrence Livermore National Laboratory, Livermore, CA, Jan. 1986).
32. A. Niiler, L. J. Kecskes, T. Kottke, P. H. Netherwood Jr., and R. F. Benck, *Ballistics Research Laboratory Report*, BRL-TR-2951 (Aberdeen Proving Ground, MD, Dec. 1988).
33. B. H. Rabin, G. E. Korth, and R. L. Williamson, *J. Am. Ceram. Soc.* **73**(7), 2156–2157 (1990).
34. J. C. LaSalvia, L. W. Meyer, and M. A. Meyers, *J. Am. Ceram. Soc.* **75**(3), 592–602 (1992).
35. D. A. Hoke, M. A. Meyers, L. W. Meyer, and G. T. Gray III, *Metall. Trans. A* **23A**, 77–86 (1992).
36. J. W. McCauley, N. D. Corbin, T. Resetar, and P. Wong, *Ceram. Eng. Sci. Proc.* **3**, 538–554 (1982).
37. D. M. Sims, A. Bose, and R. M. German, *Prog. Powd. Metall.* **43**, 575–596 (1987).
38. A. G. Merzhanov, V. I. Yukhvid, and I. P. Borovinskaya, *Dokl. Akad. Nauk SSSR* **255**(1), 503–506 (1980).
39. S. Ranganath, M. Vijayakumar, and J. Subrahmanyam, *Mater. Sci. Eng.* **A149**, 253–257 (1992).
40. E. R. Stover and J. Wulff, *Trans. Metall. Soc. AIME* **215**, 127–136 (1959).
41. V. M. Gorokhov, M. S. Koval'chenko, and O. V. Roman, *Sov. Powder Metall. Meta. Ceram.* **149**(9), 708–712 (1983).
42. B. L. Ferguson, A. Kuhn, O. D. Smith, and A. Hofstatter, in *Powder Metallurgy for Full Density Products, New Perspectives in Powder Metallurgy: 8*, K. M. Kulkarni, ed. (Metal Powder Industries Federation, Princeton, NJ, 1987), pp. 225–236.
43. I. P. Borovinskaya, E. A. Levashov, and A. S. Rogachev, *Physical-Chemical and Technological Base of Self-Propagating High-Temperature Synthesis: Course of Lectures* (Scientific-Educational Center of SHS, Moscow, 1991).
44. A. S. Rogachev, V. M. Shkiro, I. D. Chausskaya, and M. V. Shvetsov, *Combust. Explos. Shock Waves* **24**(6), 720–726 (1988).
45. J. C. LaSalvia, Master's Thesis (University of California, San Diego, La Jolla, 1990).
46. J. Wong, E. M. Larson, J. B. Holt, P. A. Waide, B. Rupp, and R. Frahm, *Science* **249**, 1406–1409 (1990).
47. W. F. Henshaw, A. Niiler, and T. Leete, Memorandum Report, ARBRL-MR-03354 (Aberdeen Proving Ground, MD, April 1984).
48. Ya. B. Zeldovich, G. I. Barenblatt, V. B. Librovich, and G. M. Makhviladze, *The Mathematical Theory of Combustion and Explosions* (Consultants Bureau, New York, 1985).
49. V. M. Maslov, S. S. Mamyan, and S. I. Voyuev, *Combust. Explos. Shock Waves* **19**(5), 634–637 (1983).
50. V. N. Bloshenko, V. A. Bokii, and I. P. Borovinskaya, *Combust. Explos. Shock Waves* **20**(6), 673–675 (1984).
51. M. Humenik Jr. and N. M. Parikh, *J. Am. Ceram. Soc.* **39**(2), 60–63 (1956).
52. *CRC Handbook of Chemistry and Physics*, D. R. Lide, ed. (CRC Press, Boston, 1990).
53. J. C. LaSalvia, R. A. Lipsitt, and M. A. Meyers, in press (1994).
54. R. M. German, *Liquid Phase Sintering* (Plenum Press, New York, 1986).
55. G. E. Hollox and R. E. Smallman, *J. Appl. Phys.* **37**(2), 818–823 (1966).
56. G. Das, K. S. Mazdiyasni, and H. A. Lipsitt, *J. Am. Ceram. Soc.* **65**(2), 104–110 (1982).